

This article was downloaded by:[Canadian Research Knowledge Network]
On: 19 March 2008
Access Details: [subscription number 783018834]
Publisher: Taylor & Francis
Informa Ltd Registered in England and Wales Registered Number: 1072954
Registered office: Mortimer House, 37-41 Mortimer Street, London W1T 3JH, UK



Electromagnetics

Publication details, including instructions for authors and subscription information:
<http://www.informaworld.com/smpp/title~content=t713770615>

Photonic Crystal Fiber and Waveguide-Based Surface Plasmon Resonance Sensors for Application in the Visible and Near-IR

Alireza Hassani ^a; Bertrand Gauvreau ^a; Majid Fassi Fehri ^a; Andrei Kabashin ^a; Maksim Skorobogaty ^a

^a Engineering Physics Department, École Polytechnique de Montréal, Montreal, Québec, Canada

Online Publication Date: 01 April 2008

To cite this Article: Hassani, Alireza, Gauvreau, Bertrand, Fehri, Majid Fassi, Kabashin, Andrei and Skorobogaty, Maksim (2008) 'Photonic Crystal Fiber and Waveguide-Based Surface Plasmon Resonance Sensors for Application in the Visible and Near-IR', *Electromagnetics*, 28:3, 198 - 213

To link to this article: DOI: 10.1080/02726340801921627

URL: <http://dx.doi.org/10.1080/02726340801921627>

PLEASE SCROLL DOWN FOR ARTICLE

Full terms and conditions of use: <http://www.informaworld.com/terms-and-conditions-of-access.pdf>

This article maybe used for research, teaching and private study purposes. Any substantial or systematic reproduction, re-distribution, re-selling, loan or sub-licensing, systematic supply or distribution in any form to anyone is expressly forbidden.

The publisher does not give any warranty express or implied or make any representation that the contents will be complete or accurate or up to date. The accuracy of any instructions, formulae and drug doses should be independently verified with primary sources. The publisher shall not be liable for any loss, actions, claims, proceedings, demand or costs or damages whatsoever or howsoever caused arising directly or indirectly in connection with or arising out of the use of this material.

Photonic Crystal Fiber and Waveguide-Based Surface Plasmon Resonance Sensors for Application in the Visible and Near-IR

ALIREZA HASSANI,¹ BERTRAND GAUVREAU,¹
 MAJID FASSI FEHRI,¹ ANDREI KABASHIN,¹ and
 MAKSIM SKOROBOGATIY¹

¹École Polytechnique de Montréal, Engineering Physics Department,
 Centre-Ville Montreal, Québec, Canada

Abstract *In the proposed photonic crystal waveguide-based surface plasmon resonance (SPR) sensor, a plasmon wave on the surface of a thin metal film is excited by a Gaussian-like leaky mode of an effectively single-mode photonic crystal waveguide. By judicious design of a photonic crystal waveguide, the effective refractive index of a core mode can be made considerably smaller than that of the core material, thus enabling efficient phase-matching with a plasmon, high sensitivity, and high coupling efficiency from an external Gaussian source, at any wavelength of choice from the visible to near infrared (IR), which is, to our knowledge, not achievable by any other design. Moreover, unlike the case of total internal reflection (TIR) waveguide-based sensors, a wide variety of material combinations can be used to design photonic crystal waveguide-based sensors as there is no limitation on the value of the waveguide core refractive index. This sensor design concept was implemented using planar multilayer photonic crystal waveguides, solid and hollow core Bragg fibers, as well as microstructured photonic crystal fibers. Amplitude and spectral-based methodologies for the detection of changes in the analyte refractive index were devised. Sensor resolution as low as $8.3 \cdot 10^{-6}$ refractive-index unit (RIU) was found for aqueous analyte.*

Keywords surface wave, SPR, fiber optic sensors, photonic crystal fiber

1. Introduction

Propagating at the metal/dielectric interface, surface plasmons (Agranovich & Mills, 1982) are extremely sensitive to changes in the refractive index of the dielectric. This feature constitutes the core of many SPR sensors. Typically, these sensors are implemented in the Kretschmann-Raether prism geometry where *p*-polarized light is launched through a glass prism and reflected from a thin metal (Au, Ag) film deposited on the prism facet (Kretschmann & Raether, 1968). The presence of a prism allows phase matching of an incident electromagnetic wave with a plasmonic wave at the metal/ambient dielectric

Received 2 May 2007; accepted 3 September 2007.

Address correspondence to Maksim Skorobogatiy, École Polytechnique de Montréal, Engineering Physics Department, C.P. 6079, succ., Centre-Ville Montreal, Québec H3C 3A7, Canada. E-mail: maksim.skorobogatiy@polymtl.ca

interface at a specific combination of incidence angle and wavelength. Mathematically, the phase-matching condition is expressed as an equality between the plasmon wavevector and a projection of the wavevector of an incident wave along the interface. Since the plasmon excitation condition depends resonantly on the value of the refractive index of an ambient medium within 100–300 nm from the interface, the method enables detection of biological binding events on the metal surface with unprecedented sensitivity (Liedberg et al., 1983). The course of a biological reaction can then be followed by monitoring angular (Liedberg et al., 1983; Melendez et al., 1996), spectral (Zhang & Uttamchandani, 1988), or phase (Kabashin & Nikitin, 1998; Grigorenko et al., 1999) characteristics of the reflected light. However, the high cost and large size of commercially available systems makes them useful only in a laboratory, while many important field and other applications remain out of the reach of this method.

Using optical waveguides and fibers instead of a bulk prism configuration in plasmonic sensors offers miniaturization, a high degree of integration, and a remote sensing capabilities. In fiber- and waveguide-based sensors, one launches the light into a waveguide core and then uses coupling of a guided mode with a plasmonic mode to probe for the changes in the ambient environment. To efficiently excite a surface plasmon, the phase matching condition between a plasmon and a waveguide mode has to be satisfied, which mathematically amounts to the equality between their modal propagation constants (effective refractive indices). Over the past decade, driven by the need for miniaturization of SPR sensors, various compact configurations enabling coupling between optical waveguide modes and surface plasmonic waves have been investigated. Among others, metallized single-mode, multimode, and polarization-maintaining waveguides and fibers, metallized tapered fibers, metallized fiber Bragg gratings (Vidal et al., 1993; Alonso et al., 1994; Homola, 1995; Tubb et al., 1997; Homola et al., 1997; Diez et al., 2001; Piliarik et al., 2003; Monzon-Hernandez et al., 2004; Monzon-Hernandez & Villatoro, 2006; Suzuki et al., 2006; Ctyroky et al., 1999a, 1999b; Al-Bader & Imtaar, 1993; Jorgenson & Yee, 1993; Trouillet et al., 1996; Weisser et al., 1999; Gupta & Sharma, 2005) and, recently, solid-core microstructured fibers (Kuhlmey et al., 2006; Hassani & Skorobogatiy, 2006, 2007), as well as planar photonic crystal waveguides (Skorobogatiy & Kabashin, 2006a, 2006b) have been studied. In the majority of fiber implementations (with an exception of microstructured fibers), one typically strips the fiber polymer jacket and polishes off the fiber cladding until the fiber core is exposed; then, a metal layer is coated directly onto the fiber core. Thus, the functionalized surface of a fiber core is then exposed to an analyte. Ideally, one would use a single-mode fiber or waveguide with all the power traveling in a single Gaussian-like core mode operating near the point of resonant excitation of a plasmon (Lavers & Wilkinson, 1994; Harris & Wilkinson, 1995; Weiss et al., 1996; Homola et al., 1997; Dostalek et al., 2001; Sheridan et al., 2004). A Gaussian shape for core mode is important as it is best suited for excitation by standard Gaussian laser sources. Near the point of phase matching, most of the energy launched into a waveguide core mode could be efficiently transferred into a plasmon mode. However, in the TIR single-mode waveguides with low refractive index-contrast, coupling with a plasmon is essentially realized at grazing angles of modal incidence on a metal layer. As follows from the basic SPR theory, coupling at such grazing incidence angles leads to an inevitable decrease of sensitivity of an SPR method. In principle, high index-contrast single-mode waveguides (see Figure 1(a)) could be employed to increase the angle of modal incidence on the interface. However, phase matching between plasmon and fundamental waveguide mode is typically hard to realize. This is related to the fact that the effective refractive index of a core-guided mode is

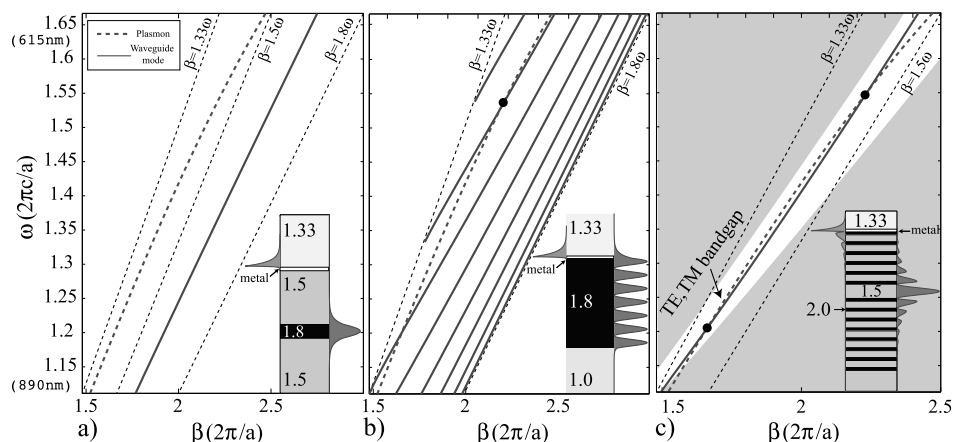


Figure 1. Band diagrams and schematics of various sensor implementations. (a) Single-mode waveguide-based sensor: dispersion relations of a core-guided mode (solid) and a plasmon (thick dashed); inset—coupler schematic; $|H_{\parallel}|^2$ of a plasmon (left) and a core mode (right). (b) Multimode waveguide-based sensor: dispersion relations of the core modes (solid) and a plasmon (thick dashed); inset—coupler schematic; $|H_{\parallel}|^2$ of a plasmon (left) and a high-order mode (right) at the phase-matching point (black circle). (c) Planar photonic crystal waveguide-based sensor: dispersion relation of a fundamental Gaussian-like leaky core mode (solid) and a plasmon (thick dashed); inset—coupler schematic; $|H_{\parallel}|$ of a plasmon (left) and a core mode (right).

close to the refractive index of the core material, which is typically larger than 1.45 due to practical material limitations. The effective refractive index of a plasmon is close to the refractive index of the ambient medium, which is typically $n_a = 1$ for air or $n_a = 1.3$ for water. Thus, a large discrepancy in the effective indices (as seen from Figure 1(a)) makes phase matching between the two modes hard to achieve, except at higher frequencies ($\lambda < 650$ nm), where the plasmon dispersion relation deviates toward higher refractive indices. Thus, due to practical limitation on the lowest value of the waveguide core and cladding refractive indices, single-mode TIR waveguide-based sensors were demonstrated mostly in the visible, where the phase-matching condition is easier to enforce.

Problems with phase matching and loss of sensitivity due to shallow angles of incidence could be, in principle, alleviated by using multimode waveguides (Jorgenson & Yee, 1993; Trouillet et al., 1996; Ctyroky et al., 1999b; Weisser et al., 1999; Gupta & Sharma, 2005) (see Figure 1(b)). If launched properly, modal effective propagation angles in such waveguides can be much steeper, resulting in smaller effective refractive indices. However, in multimode waveguides only a certain number of higher-order modes will be phase matched with a plasmon. Thus, sensitivity and stability of such sensors depend crucially on launch conditions. Moreover, as spatial field distribution in a Gaussian-like laser source is typically not well matched with the field distribution of a higher-order mode of a multimode waveguide, only a small fraction of energy can be launched into such a mode, resulting, again, in decreased sensitivity.

In this article, we present design principles of novel photonic crystal fiber and waveguide-based SPR sensors and show that they integrate advantages of both the single- and multimode waveguide-based SPR sensors. Moreover, in photonic crystal fiber and waveguide-based SPR sensors, fundamental Gaussian-like leaky core modes

(see Figure 1(c)) can be phase matched with a plasmon at any desired wavelength of operation, thus enabling sensing anywhere from the visible to mid-IR. The term “leaky mode” generally refers to the guidance mechanism, where the effective refractive index of a propagating mode is smaller than that of the waveguide cladding. Such unusual modes are called leaky modes as, outside of a waveguide core, they do not exhibit a traditional evanescent decay into the cladding, but rather they radiate slowly (leak) into the cladding. Unlike in the case of common TIR waveguides, leaky modes in photonic crystal waveguides are confined by the bandgap of a photonic crystal reflector. As a consequence, the effective refractive index of the fundamental (lowest loss) leaky core mode can be designed to be arbitrarily smaller than that of a waveguide core material, thus enabling phase matching with a plasmon at any desired frequency. Moreover, the lowest loss leaky core mode typically exhibits a Gaussian-like intensity distribution in the waveguide core region, thus enabling convenient excitation by a Gaussian beam of an external light source. Using the fundamental (lowest loss) leaky mode for sensing gives the additional advantage of an effectively single-mode propagation regime. In particular, when a set of modes is excited at a sensor input, higher-order leaky modes radiate out faster than a fundamental mode. Consequently, after a certain propagation distance, only the fundamental mode is left in the waveguide core. Finally, the effective angle of modal incidence onto a metal film, and hence sensitivity, can be varied, at will, by a proper selection of the waveguide core and reflector materials.

The article is organized as follows. In the first part, we introduce planar photonic crystal waveguide-based SPR sensors and highlight the key ideas for their design. In the second part, we demonstrate the design of SPR sensors using solid-core and analyte-filled hollow-core Bragg fibers operating at 685 nm, 850 nm, and 1,300 nm. We argue that for plasmon excitation in the near-IR, the analyte-filled hollow-core Bragg fibers present a potent solution for plasmon excitation. In the third part of the article, we present an SPR sensor using honeycomb microstructured photonic crystal fiber operating at 1,000 nm. We conclude by summarizing major findings of this paper.

Finally, throughout the article, to find the modes of planar waveguides and circular symmetric Bragg fibers, we have used a standard transfer matrix approach; while for the calculation of modes of microstructured fibers, we have used commercial finite element code by Rsoft.

2. SPR Sensors Using Planar Photonic Crystal Waveguides

We start by considering plasmon excitation by a Gaussian-like transverse-magnetic (TM)-polarized mode of a planar photonic crystal waveguide (see Figure 2(a)), in which light confinement in a lower refractive index core is achieved by a surrounding multilayer reflector. TM polarization of the electromagnetic field in a planar multilayer assumes a single magnetic field component, H_{\parallel} , directed parallel to the plane of a multilayer, while the electric field component is confined to a plane perpendicular to the multilayer. The photonic crystal waveguide under consideration consists of 27 alternating layers, having refractive indices $n_h = 2.0$ and $n_l = 1.5$. The core layer is layer number 12, having refractive index $n_c = n_l$. Analyte (first cladding) is water $n_a = 1.332$ bordering a 50-nm layer of gold. The substrate refractive index is 1.5. Theory of planar photonic crystal waveguides with infinite reflectors, where $n_c = n_l$ (Skorobogatiy, 2005), predicts that, for a design wavelength λ_c , the effective refractive index $n_{eff}(\lambda_c)$ of the fundamental transverse-electric (TE)- and TM core-guided modes can be designed at will, as long as

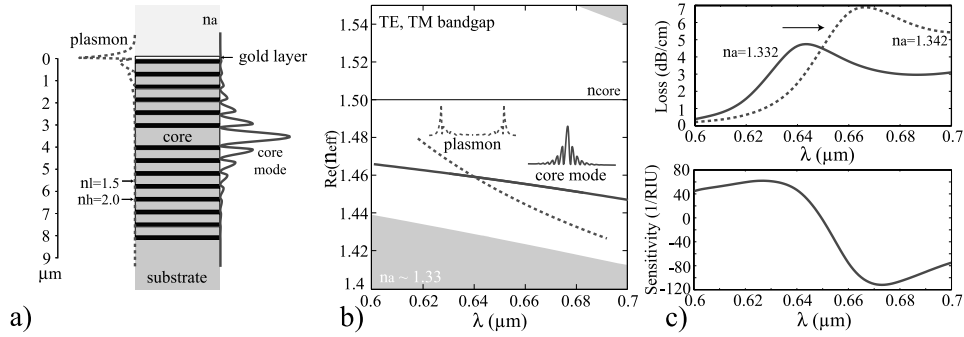


Figure 2. Planar photonic crystal waveguide-based SPR sensor. (a) Schematic of a sensor where the low-refractive index core is surrounded by the periodic photonic crystal reflector. One side of the reflector is gold-plated for plasmon excitation. The gold layer is bordered by an aqueous analyte. The $|H_{\parallel}|$ field distribution in the fundamental core mode is shown on the right, while field distribution in a plasmonic mode is shown on the left of the sensor schematic. (b) Band diagram of sensor modes showing dispersion relation and field distribution of the fundamental core mode (thick solid curve) and plasmonic mode (dashed curve). The common part of the TE and TM bandgaps of a periodic reflector is shown as a clear region, while gray regions correspond to the continuum of the bulk reflector states. By design, the effective refractive index of a core-guided mode can be made significantly smaller than that of the waveguide core material. (c) Upper part: the solid curve shows the loss of a waveguide core mode near the phase-matching point with a plasmon at which modal loss peaks. The dashed line shows the shift of the modal loss curve when the refractive index of the analyte is varied. Lower part: dependence of the sensor amplitude sensitivity on wavelength.

$0 \leq n_{eff} < n_l$, by choosing the reflector layer thicknesses as

$$d_{l,h} = \frac{\lambda_c}{4\sqrt{n_{l,h}^2 - n_{eff}^2(\lambda_c)}}, \quad (1)$$

and by choosing the core layer thickness as $d_c = 2d_l$. Moreover, for this choice of n_c , the field distribution in the core is always Gaussian-like for TE-polarized modes, while for TM-polarized modes, it is Gaussian-like as long as $n_{eff}^2 > \epsilon_l \epsilon_h / (\epsilon_l + \epsilon_h)$ (Skorobogatiy, 2005). By choosing the effective refractive index of a core mode to be that of a plasmon, a desired phase-matching condition is achieved. For a waveguide with a finite reflector, the same design principle holds approximately. Thus, for an operating wavelength of $\lambda = 640$ nm considered in this example, phase matching is achieved when the photonic crystal waveguide above is designed using $\lambda_c = 635$ nm and $n_{eff}(\lambda_c) = 1.46$. A reasonable approximation to the $n_{eff}(\lambda_c)$ is a value of the effective refractive index of a plasmonic wave, propagating at a planar gold-analyte interface

$$n_{eff}^2(\lambda_c) = \frac{\epsilon_{gold}(\lambda_c)\epsilon_a(\lambda_c)}{\epsilon_{gold}(\lambda_c) + \epsilon_a(\lambda_c)}, \quad (2)$$

where ϵ_a is the dielectric constant of an analyte, and ϵ_{gold} is the dielectric constant of the gold layer approximated by the Drude model

$$\epsilon_{gold} = \epsilon_{\infty} - \frac{(\lambda/\lambda_p)^2}{1 + i(\lambda/\lambda_t)}, \quad (3)$$

where the choice $\epsilon_\infty = 9.75$, $\lambda_t = 13.0 \mu\text{m}$, $\lambda_p = 0.138 \mu\text{m}$ presents one of the many possible fits of the experimental data.

In Figure 2(b), we present a band diagram of a planar photonic crystal waveguide-based SPR sensor. All the simulations are performed using standard transfer matrix theory on a complete system that includes both the waveguide and metal layer. Gray regions signify bulk states of a periodic reflector. The clear region is a common part of the reflector TE and TM bandgaps. The thick solid line, which is almost parallel to the band gap edges, marked as “core mode” is a dispersion relation of a Gaussian-like leaky core mode with most of its modal energy concentrated in the low-refractive index core. The dashed line marked as “plasmon” represents the dispersion relation of a plasmonic mode. Most of the plasmon energy is concentrated at the metal/analyte interface.

Near the phase-matching point, fields of a core-guided mode contain strong plasmonic contribution. As the plasmon exhibits very high propagation loss, the loss of a core mode (upper plot in Figure 2(c)) will also exhibit a sharp increase near the phase-matching point. An important aspect of the proposed setup is the freedom of adjusting loss of the core mode. As a leaky mode decays exponentially with respect to distance into the multilayer reflector, coupling strength between the plasmon and core modes can be controlled by changing the number of reflector layers situated between the waveguide core and a metal film. Ultimately, higher coupling strength leads to higher modal losses, hence, shorter sensor length. When the real part of the analyte refractive index is varied, the plasmon dispersion relation displaces accordingly, thus leading to a shift in the position of the phase-matching point with a core-guided mode. Consequently, in the vicinity of the phase-matching point, transmission loss of a core-guided mode varies strongly with changes in the analyte refractive index (see the upper part of Figure 2(c)).

We would like to point out that what is identified as a “core mode” in all the figures in this article is, in fact, a waveguide supermode that includes both the core-guided mode and plasmonic contribution. Since the plasmon mode is extremely lossy, only a small mixing of this mode with the core mode is necessary to achieve sensing. We found it pertinent to also show on the graphs what a plasmonic mode looks like near the phase-matching point, although this mode by itself is not used in our sensing arrangements. Depending on the designs, the plasmon contribution to the evanescent tail of a core mode is not always visible on the field distribution plots as only the real components of the modes are truly phase matched.

The simplest mode of operation of a waveguide-based SPR sensor is detection of small changes in the bulk refractive index of an analyte. There are two main modalities of SPR detection—amplitude-based and spectral-based. In both methodologies, sensing is enabled through detection of changes in the location of a sharp plasmonic loss peak, where spectral position is strongly dependent on the value of the ambient refractive index. In the amplitude-based approach, all the amplitude measurements are performed at a single wavelength near the center of a plasmonic peak. The advantage of this method is its simplicity and low cost, as no spectral manipulation is required. The disadvantage is a smaller dynamic range and lower sensitivity when compared to the wavelength interrogation approach, in which the whole transmission spectra are taken and compared before and after the change in the analyte has occurred.

We start by describing a single wavelength, amplitude-based detection method. We define $\alpha(\lambda, n_a)$ to be the transmission loss of a core mode as a function of the wavelength and refractive index of an analyte n_a . Considering P_0 to be the power launched into the fiber core mode, the power detected after propagation along the sensor of length L will be $P(L, \lambda, n_a) = P_0 \exp(-\alpha(\lambda, n_a)L)$. For the operating wavelength λ ,

amplitude sensitivity to the small changes in the analyte refractive index Δn_a can then be defined (and measured) as $S_A(\lambda)[\text{RIU}^{-1}]|_{\Delta n_a \rightarrow 0} = (P(L, \lambda, n_a + \Delta n_a) - P(L, \lambda, n_a)) / P(L, \lambda, n_a) / \Delta n_a$. Sensor length L is typically limited by the modal transmission loss. A reasonable choice of a sensor length is $L = 1/\alpha(\lambda, n_a)$, which is ~ 1 cm range for the planar multilayer-based sensor described in this section. Such a choice of sensor length results in a simple definition of sensitivity for the small changes in the analyte refractive index

$$S_A(\lambda)[\text{RIU}^{-1}] = \frac{1}{P(L, \lambda, n_a)} \frac{\partial P(L, \lambda, n_a)}{\partial n_a} = -\frac{1}{\alpha(\lambda, n_a)} \frac{\partial \alpha(\lambda, n_a)}{\partial n_a}. \quad (4)$$

In the lower part of Figure 2(c), we present the amplitude sensitivity of the proposed planar photonic crystal waveguide-based SPR sensor. Maximal sensitivity is achieved at 673 nm and is equal to 112 RIU^{-1} . It is typically a safe assumption that 1% change in the transmitted intensity can be detected reliably, which leads to a sensor resolution of $8.9 \cdot 10^{-5} \text{ RIU}$. This 1% criterion will be used throughout the article to compare the sensors response.

In the wavelength interrogation mode, changes in the analyte refractive index are detected by measuring displacement of a plasmonic peak λ_{peak} . In this case, sensitivity is defined as

$$S_\lambda[\text{nm} \cdot \text{RIU}^{-1}] = \frac{d\lambda_{peak}(n_a)}{dn_a}. \quad (5)$$

In the case of a planar photonic crystal waveguide-based SPR sensor, we find that the corresponding spectral sensitivity is $2,300 \text{ nm} \cdot \text{RIU}^{-1}$. Assuming that a 0.1 nm change in the position of a resonance peak can be detected reliably, a sensor resolution of $4.3 \cdot 10^{-5} \text{ RIU}$ is obtained. The sensor length in this case is ~ 1 cm.

3. SPR Sensors Using Photonic Crystal Bragg Fibers

In this section, we propose two distinct approaches for fiber-based SPR sensing in aqueous solutions using photonic crystal Bragg fibers. In both cases, a thin, gold layer is deposited on the outer surface of a Bragg fiber in direct contact with an analyte. By tailoring the dispersion relation of the fundamental core-guided mode of a Bragg fiber, the phase-matching condition is obtained at various wavelengths in the visible and near-IR.

3.1. Large Solid-Core Bragg Fiber-Based Sensor

The first design approach consists of using the leaky fundamental Gaussian-like core mode of a Bragg fiber and lowering its effective refractive index toward that of a plasmon by the proper choice of a fiber reflector and a fiber core size. The choice of the fundamental Gaussian-like core mode over the higher-order modes is motivated by its optimal spatial overlap with the common Gaussian laser sources. Moreover, when a sufficiently long Bragg fiber is used, effective single-mode regime of operation can be achieved by radiation of higher-order modes, thus reducing the overall noise limit of a sensor. In particular, we consider solid-core photonic crystal Bragg fibers made of two materials with refractive indices $n_l = 1.40$ and $n_h = 1.60$. Prototypes of such fibers have been recently fabricated in our group by using a poly(vinylene difluoride)/polycarbonate (PVDF/PC) and poly(methyl methacrylate)/polystyrene (PMMA/PS) material combinations (Gao et al., 2006). In such fibers, the solid core of refractive index n_l is surrounded

by N alternating high- and low-refractive index reflector layers of thicknesses d_l and d_h . A typical choice of the reflector layer thicknesses is in accordance with the quarter wave relation Eq. (1), where λ_c defines the center wavelength of the Bragg reflector bandgap, and $n_{eff}(\lambda_c)$ is the desired effective refractive index of a core mode at that wavelength. This choice of the reflector parameters only guarantees efficient bandgap guidance at λ_c of a mode with effective refractive index $n_{eff}(\lambda_c)$; however, it does not guarantee the existence of such a mode. As it will be detailed in what follows, one effective way of positioning a core mode dispersion relation inside of a fiber bandgap is by varying the fiber core diameter d_c . In a large-core diameter Bragg fiber where $d_c \gg \lambda_c$, the effective refractive index of the fundamental core mode is close to that of a core material. By decreasing the fiber core size, one can considerably reduce the core mode effective refractive index.

With the choice of a desired phase matching λ_c and an approximation of the $n_{eff}(\lambda_c)$ performed using Eq. (2), we are still left with two free parameters, which are the number of layers N in a Bragg reflector and the fiber core size d_c . In metallized Bragg fibers, guided modes incur additional losses due to high absorption of the metal film. When operating within the bandgap of a Bragg fiber, fields of a leaky core mode decay exponentially fast into the periodic reflector. Thus, modal presence in the metallized region also decreases exponentially with the number of reflector layers. From this, we conclude that variation in the number of reflector layers will primarily effect the core mode propagation loss.

We now investigate, in more detail, the effect of core size on the modal structure of an SPR sensor. First, we consider a Bragg fiber sensor having a large-core diameter, $d_c = 8 \mu\text{m}$, operating in the vicinity of $\lambda_c = 740 \text{ nm}$, and featuring a four-layer reflector plated with a 40-nm thick layer of gold (see Figure 3(a)). Reflector layer thicknesses

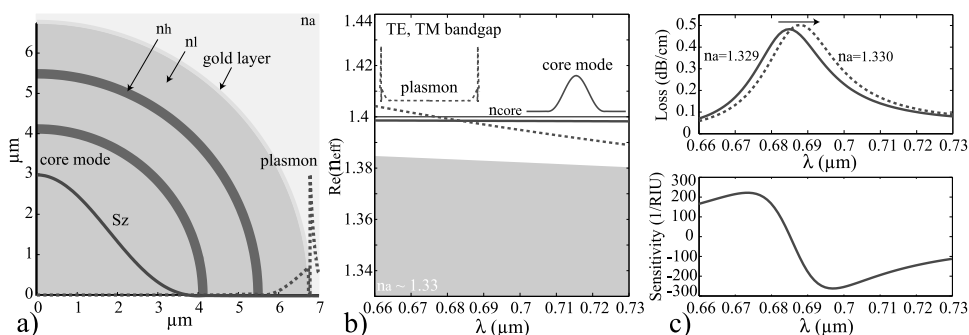


Figure 3. Large solid-core photonic crystal Bragg fiber-based SPR sensor. (a) Schematic of a sensor where the low-refractive index core is surrounded by a concentric photonic crystal reflector. Outside, the reflector is gold-plated for plasmon excitation. The gold layer is bordered by an aqueous analyte. Energy flux distribution across the fiber cross-section is shown with a solid curve for the fundamental core mode and a dashed curve for the plasmonic mode. (b) Band diagram of sensor modes showing dispersion relation and field distribution of the fundamental core mode (thick solid curve) and plasmonic mode (dashed curve). The common part of the TE and TM bandgaps of a periodic planar reflector is shown as a clear region, while gray regions correspond to the continuum of the bulk reflector states. (c) Upper part: the solid curve shows the loss of the fundamental core mode near the phase-matching point with a plasmon at which modal loss peaks. The dashed line shows the shift of the modal loss curve when the refractive index of an analyte is varied. Lower part: dependence of the sensor amplitude sensitivity on wavelength.

are chosen to be $d_l = 1,133$ nm and $d_h = 235$ nm. In Figure 3(b), we present the band diagram of this defined Bragg fiber sensor. Common TM and TE bandgaps of a corresponding infinitely periodic Bragg reflector is presented as a clear region, while gray regions signify a continuum of the reflector bulk states. For a large-core photonic crystal Bragg fiber, the effective refractive index of the lowest loss leaky mode (thick solid line) is close to that of the refractive index of a core material (thin solid line). The dispersion relation of a plasmon mode is shown as a thick dashed line. The dispersion relations of the core-guided and plasmonic modes near λ_c are positioned well inside the reflector band gap by its proper design. Therefore, the fundamental core mode (solid curve in Figure 3(a)) is well confined within the Bragg fiber core, while the plasmon mode (dashed curve in Figure 3(a)) is mostly confined to the metal coating and the last reflector layer. Phase matching between the core and plasmonic modes is achieved at $\lambda = 684$ nm.

In the upper plot of Figure 3(c), propagation loss of a core mode is presented as a function of wavelength. As seen from this figure, core mode propagation loss peaks at the wavelength of phase matching with the plasmon mode due to an efficient energy transfer from the core mode into the highly absorbing plasmon. In the lower part of Figure 2(c), we present amplitude sensitivity (Eq. (4)) of the proposed large solid-core Bragg fiber-based SPR sensor. Maximal sensitivity is achieved at 697 nm and is equal to $262 \cdot \text{RIU}^{-1}$. The sensor resolution reaches $3.8 \cdot 10^{-5}$ RIU based on the last section assumption. In the case of a large solid-core Bragg fiber-based SPR sensor, we find that the corresponding spectral sensitivity (Eq. (5)) is $3,000 \text{ nm} \cdot \text{RIU}^{-1}$. For a wavelength-based detection, a sensor resolution of $3.3 \cdot 10^{-5}$ RIU is obtained. Sensor length in this case is ~ 10 cm.

3.2. Small Solid-Core Bragg Fiber-Based Sensor

In the second design, we explore the possibility of considerably reducing the effective refractive index of a core mode by reducing the fiber core size. This enables plasmonic excitation at longer wavelengths in the near-IR. Thus, with the same overall structure of the Bragg reflector as in the prior case, by reducing the fiber core diameter to $d_c = 2.2 \mu\text{m}$, plasmonic excitation at the interface with aqueous analyte is demonstrated at 836 nm. In Figure 4(a), we show the cross-section of a small solid-core photonic crystal Bragg fiber sensor and the energy flux distributions in its leaky fundamental core mode and plasmonic mode. Although reflector layer thicknesses are the same as in the prior case (see Figure 3(a)), the total number of layers is increased to ten in order to reduce core mode radiation loss. In Figure 4(b), we present the band diagram for this design. Common TM and TE bandgaps of a corresponding infinitely periodic Bragg reflector is presented as a clear region, while gray regions signify the continuum of reflector bulk states. In a small-core photonic crystal Bragg fiber, effective refractive index of the lowest loss leaky mode (thick solid line) can be considerably smaller than the refractive index of the core bulk material (thin solid line). The dispersion relation of the plasmon mode is shown as thick dashed line. Moreover, the dispersion relation of the core-guided mode is shifted toward the lower edge of the reflector bandgap. Therefore, the core mode (solid curve in Figure 4(a)) and plasmonic mode (dashed curve in Figure 4(a)) are not strongly confined, penetrating significantly into the reflector region. Phase matching between the core and plasmonic modes is achieved at $\lambda = 836$ nm.

In the upper plot of Figure 4(c), propagation loss of the core mode is presented as a function of the wavelength. As seen from this figure, it peaks at the wavelength of

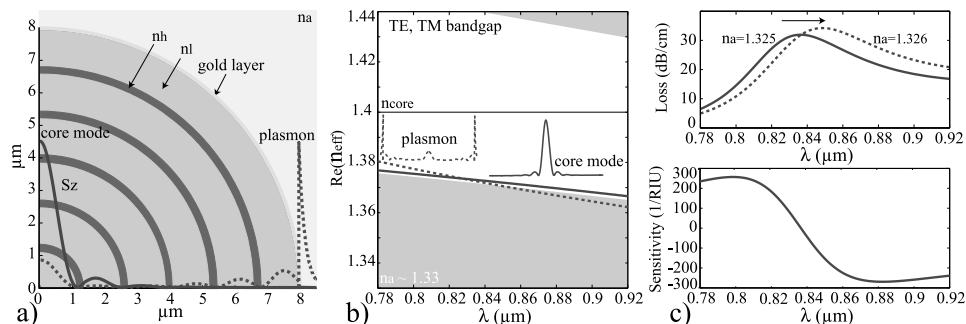


Figure 4. Small solid-core photonic crystal Bragg fiber-based SPR sensor. (a) Schematic of a sensor where the low-refractive index core is surrounded by a concentric photonic crystal reflector. Outside, the reflector is gold-plated for plasmon excitation. The gold layer is bordered by an aqueous analyte. Energy flux distribution across the fiber cross-section is shown with a solid curve for the fundamental core mode and with a dashed curve for the plasmonic mode. (b) Band diagram of sensor modes showing dispersion relation and field distribution of the fundamental core mode (thick solid curve) and plasmonic mode (dashed curve). The common part of the TE and TM bandgaps of a periodic planar reflector is shown as a clear region, while gray regions correspond to the continuum of the bulk reflector states. (c) Upper part: solid curve shows the loss of the fundamental core mode near the phase-matching point with a plasmon at which modal loss peaks. The dashed line shows the shift of the modal loss curve when the refractive index of an analyte is varied. Lower part: dependence of the sensor amplitude sensitivity on wavelength.

phase matching with the plasmon mode. In the lower part of Figure 4(c), we present amplitude sensitivity (Eq. (4)) of the proposed small solid-core Bragg fiber-based SPR sensor. Maximal sensitivity is achieved at 882 nm and is equal to $269 \cdot \text{RIU}^{-1}$. An amplitude interrogation yields a sensor resolution of $3.7 \cdot 10^{-5} \text{ RIU}$. Finally, we find that the corresponding spectral sensitivity (Eq. (5)) is $12,000 \text{ nm} \cdot \text{RIU}^{-1}$, leading to a resolution of $8.3 \cdot 10^{-6} \text{ RIU}$. Sensor length in this case is sub-cm.

3.3. Analyte-Filled Hollow-Core Bragg Fiber-Based Sensor

When designing fiber-based SPR sensors in the near-IR, one faces the difficult problem of phase matching a plasmon and a core-guided mode. The reason for such a difficulty is that, in this spectral region, the effective refractive index of a plasmon becomes very close to that of an analyte, which, for aqueous solutions, for example, is $n_a \sim 1.32$. As described in the previous section, to lower the effective refractive index of a core-guided mode to that of a plasmon, one can use a small solid-core Bragg fiber with a properly positioned bandgap region. In that case, however, fiber core size becomes too small for convenient coupling. To resolve this problem, we suggest using a large analyte-filled hollow-core Bragg fiber, as shown in Figure 5(a). In this case, as described earlier, the effective refractive index of the core mode (thick solid line in Figure 5(b)) is close, and somewhat smaller than, the refractive index of the core material (analyte). In turn, the plasmon refractive index (dashed line in Figure 5(b)) is close, and somewhat larger than, the refractive index of the analyte. To enable phase matching between the core mode and a plasmon, one has to force the core mode to cross over the dispersion relation of an analyte. As detailed in Engeness et al. (2003), to force such a crossing, one has to introduce a defect into the structure of a reflector so as to induce anticrossing of the core

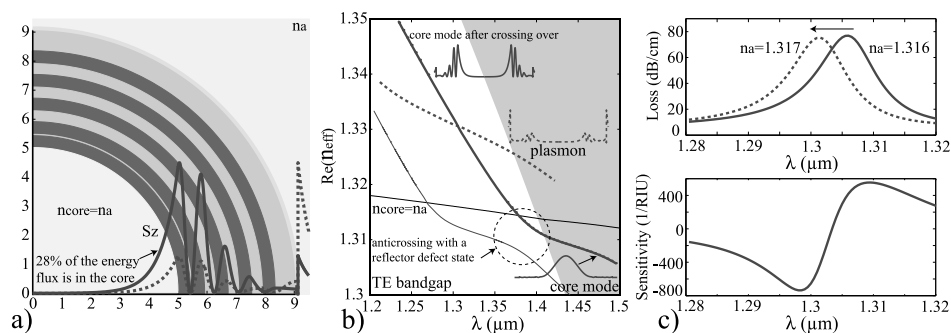


Figure 5. Analyte-filled large hollow-core photonic crystal Bragg fiber-based SPR sensor. (a) Schematic of a sensor where the analyte-filled hollow-core is surrounded by a concentric photonic crystal reflector. Outside, the reflector is gold-plated for plasmon excitation. The gold layer is bordered by an aqueous analyte. The energy flux distribution across the fiber cross-section is shown with a solid curve for the fundamental core mode and a dashed curve for the plasmonic mode. (b) Band diagram of sensor modes showing dispersion relation of the fundamental core mode crossing over the analyte light line (thick solid curve) and plasmonic mode (dashed curve). The TE bandgap of a periodic planar reflector is shown as a clear region, while gray regions correspond to the continuum of the bulk reflector states. (c) Upper part: solid curve shows the loss of the crossed-over core mode near the phase-matching point with a plasmon at which modal loss peaks. The dashed line shows the shift of the modal loss curve when refractive index of an analyte is varied. Lower part: dependence of the sensor amplitude sensitivity on wavelength.

mode with a reflector defect state (marked as a dashed circular region in Figure 5(b)). The particular sensor geometry implementing this design principle is presented in Figure 5(a). In this sensor, analyte-filled fiber core of diameter $d_c = 10 \mu\text{m}$ is surrounded by a ten-layer reflector with alternating refractive indices $n_l = 1.4$ and $n_h = 1.6$. All the low-refractive index layers, with the exceptions of the second and tenth layers, have thicknesses $d_l = 373 \text{ nm}$, while all the high-refractive index layers have thicknesses of $d_h = 435 \text{ nm}$. On the outside, the reflector is plated with a 40-nm gold layer. Two defects are incorporated into the structure of the Bragg reflector. The first defect is introduced into the outer layer by doubling its thickness to 870 nm. This defect is introduced to get rid of an unwanted surface state on the fiber-metal-analyte interface. The second defect is introduced into the second layer by reducing its thickness to 47 nm. The high-refractive index defect created by the first three layers of the reflector attracts a localized state that causes anticrossing with the core mode, thus forcing the core mode to cross over the dispersion relation of the analyte and enabling phase matching with a plasmon.

The main disadvantage of this plasmon excitation mechanism is that the intensity distribution in a crossed-over core mode stops being Gaussian-like. In fact, such a mode is evanescent in the analyte region; hence, it becomes somewhat difficult to excite with a common Gaussian laser source. However, when the plasmon dispersion relation is very close to that of the analyte (as it is the case in the near-IR), then the evanescent tail of a crossed-over core mode can extend substantially into the analyte-filled core region, thus considerably simplifying coupling to such a mode. For example, the design of Figure 5(a) enables phase matching with a plasmon near 1,306 nm (as seen from Figure 5(b)). At this wavelength, a crossed-over core mode still has 28% of its energy concentrated in the analyte-filled hollow-fiber core.

We conclude with sensitivity analysis of the proposed near-IR SPR sensor. In the lower part of Figure 5(c), we present sensor amplitude sensitivity (Eq. (4)). Maximal sensitivity is achieved at 1,298 nm and is equal to $725 \cdot \text{RIU}^{-1}$. Once again, assuming that a 1% change in the transmitted intensity can be detected reliably, leads to a sensor resolution of $1.4 \cdot 10^{-5}$ RIU. Finally, we find that the corresponding spectral sensitivity (Eq. (5)) is $4,300 \text{ nm} \cdot \text{RIU}^{-1}$. A spectral interrogation leads to a sensor resolution of $2.3 \cdot 10^{-5}$ RIU. Sensor length in this case is sub-cm.

4. SPR Sensors Using Microstructured Photonic Crystal Fibers

In the previous section, we presented several design strategies for the SPR sensors based on photonic crystal Bragg fibers. In principle, any photonic bandgap fiber can be used in place of a Bragg fiber to develop such sensors. In this section, we present an example of an SPR sensor based on a solid-core honeycomb photonic crystal fiber. As core guiding in such a fiber is analogous to core guiding in a small solid-core Bragg fiber discussed earlier, our presentation will be brief. In Figure 6(a), the schematic of a honeycomb photonic crystal fiber-based SPR sensor is presented. Design parameters are chosen as follows: the center-to-center distance between adjacent holes is $\Lambda = 1.33 \mu\text{m}$, the cladding hole diameter is $d = 0.6\Lambda$, and the diameter of the hole in the core center is $d_c = 0.45\Lambda$. The central hole in the fiber core lowers its effective refractive index compared to that of a silica cladding. The fiber is made of silica glass with refractive index $n_{\text{glass}} = 1.45$, the core and cladding holes are filled with air $n_{\text{air}} = 1$, while the large semi-circular channels are plated with an $\sim 40\text{-nm}$ thick layer of gold and filled with aqueous analyte $n_a \sim 1.33$. With these parameters, the fiber core supports a leaky core mode confined by the bandgap of the honeycomb reflector. Guided by the bandgap of the fiber reflector, core mode effective refractive index can be considerably lower than that of

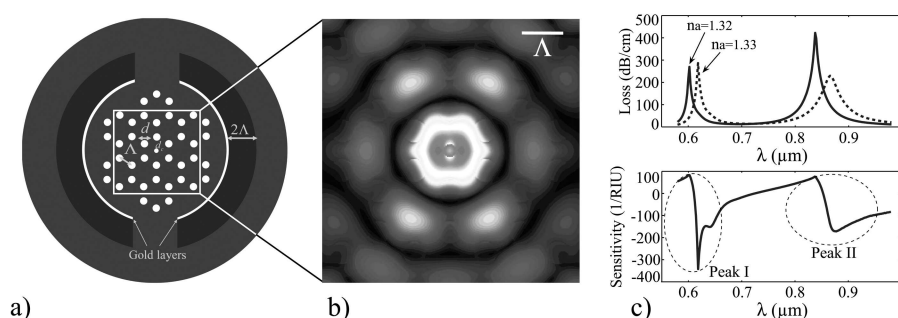


Figure 6. Solid-core honeycomb photonic crystal fiber-based SPR sensor. (a) Schematic of a sensor where the solid-core, having a small central hole, is surrounded by a honeycomb photonic crystal reflector. Two large channels are integrated to implement analyte access to the fiber reflector region. Channels are gold-plated for plasmon excitation. The gold layer is bordered by an aqueous analyte. The purpose of the ring surrounding the channels is to add mechanical rigidity to the fiber and enable microfluidic manipulations. (b) Energy flux distribution across the fiber cross-section is shown for the fundamental core mode. (c) Upper part: the solid curve shows the loss of the fundamental core mode near the phase-matching point with a plasmon at which modal loss peaks. The dashed line shows the shift of the modal loss curve when the refractive index of an analyte is varied. Lower part: dependence of the sensor amplitude sensitivity on wavelength.

the silica material. In addition, similar to the case of a photonic crystal Bragg fiber, radiation loss of the bandgap-guided core mode can be reduced by adding more layers to the honeycomb reflector. The main reason why we chose a honeycomb structure of the fiber reflector is because it enables a large photonic bandgap (Murao et al., 2006; Barkou et al., 1999), thus simplifying phase matching of the core-guided and plasmonic modes.

Unlike planar metal/dielectric interface that supports a single plasmonic excitation, metallized microstructured fibers can support multiple plasmonic modes (Hassani & Skorobogatiy, 2006, 2007). Thus, when tracking losses of a core-guided mode as a function of wavelength, one typically observes several plasmonic peaks corresponding to the points of phase matching between the core mode and various plasmonic modes. In principle, simultaneous detection of changes in several plasmonic peaks can improve sensor sensitivity. For the case of a honeycomb photonic crystal fiber-based sensor we observe two plasmonic peaks (see the upper part of Figure 6(c)): one located at 600 nm and another at 840 nm. In the lower part of Figure 6(c), we present amplitude sensitivity of the sensor as defined by Eq. (4). Maximal amplitude sensitivity (Eq. (4)) at the first peak is $340 \cdot \text{RIU}^{-1}$, while at the second peak it is $170 \cdot \text{RIU}^{-1}$. Based on the same 1% criterion, the sensor resolutions at the two peaks are $2.9 \cdot 10^{-5}$ RIU and $5.9 \cdot 10^{-5}$ RIU, respectively. Finally, spectral resolutions, as defined by Eq. (5) at the two peaks, are $1,600 \text{ nm} \cdot \text{RIU}^{-1}$ and $2,800 \text{ nm} \cdot \text{RIU}^{-1}$. The proper detection of a 0.1-nm change in the position of a resonance peak yields sensor resolutions at the two peaks of $6.3 \cdot 10^{-5}$ RIU and $3.6 \cdot 10^{-5}$ RIU, respectively. Sensor lengths in both cases is sub-mm.

5. Conclusion

In conclusion, we have presented a novel approach to design a waveguide-based SPR sensor, where the Gaussian-like mode of an effectively single mode photonic crystal waveguide is phase matched at any desirable wavelength to a surface plasmon propagating along the metallized part of such a waveguide. The operating wavelength of such sensors can be anywhere from the visible to near-IR. Moreover, a wide variety of material combinations can be used to design such a sensor as there is no limitation on the value of the waveguide core refractive index. Finally, coupling strength between the waveguide core and plasmon modes can be varied by changing the number of the intermediate reflector layers, which also permits designing the overall sensor length.

The methodology for the photonic crystal waveguide-based SPR sensor design is quite general, and its particular implementation can be based on metal-plated planar integrated photonic crystal waveguides, Bragg fibers or microstructured photonic crystal fibers. In particular, one starts with a choice of an operational wavelength λ_c . Then, the plasmon effective refractive index $n_{\text{eff}}(\lambda_c)$ at λ_c is approximated by its value for the plasmon excitation on a planar metal-analyte interface (Eq. (2)). Then, the photonic bandgap of a waveguide reflector at λ_c is designed to be centered in the vicinity of $n_{\text{eff}}(\lambda_c)$. By varying the waveguide core size (or by varying the geometry of a core), one can shift the dispersion relation of a core mode toward that of a plasmonic mode until phase matching occurs at λ_c . Sensor length can be changed by varying the number of layers in a photonic crystal reflector, with more efficient reflectors resulting in the longer sensors.

Finally, we have presented examples of the aqueous SPR sensors based on the planar photonic crystal waveguide, solid-, and analyte-filled Bragg fibers, as well as solid-core

microstructured photonic crystal fiber. Amplitude sensitivity of the proposed designs was as high as $725 \cdot \text{RIU}^{-1}$. Assuming that a 1% change in the transmitted intensity can be detected reliably, sensor resolution as low as $1.38 \cdot 10^{-5}$ RIU was demonstrated. Spectral sensitivity of the proposed designs was as high as $12,000 \text{ nm} \cdot \text{RIU}^{-1}$. Assuming that a 0.1-nm change in the position of a plasmonic peak can be detected reliably, sensor resolution as low as $8.3 \cdot 10^{-6}$ RIU was demonstrated. Sensor lengths in our examples varied from sub-mm to ~ 10 cm. For measuring changes in the aqueous analyte, sensitivities of our fiber designs are comparable to, or even surpass, those of the best existing waveguide-based sensor designs (Homola et al., 1999).

Acknowledgments

This work is supported in part by the Canada Institute for Photonic Innovations grants BP5 and FP3, Canada Research Chair program, and NSERC Strategic grant “Miniaturized Si-based plasmonics platform for gas detection.”

Alireza Hassani and Bertrand Gauvreau contributed equally to this article (homepage: www.photonics.phys.polymtl.ca).

References

- Agranovich, V. M., & D. L. Mills. 1982. *Surface polaritons: Electromagnetic waves at surfaces and interfaces*, V. M. Agranovich & D. L. Mills, eds., Amsterdam: North-Holland.
- Al-Bader, S. J., & M. Imtaar. 1993. Optical fiber hybrid-surface plasmon polaritons. *J. Opt. Soc. Am. B* 10:83–88.
- Alonso, R., J. Subias, J. Pelayo, F. Villuendas, & J. Tornos. 1994. Single-mode, optical fiber sensors and tunable wavelength filters based on the resonant excitation of metal-clad modes. *Appl. Opt.* 33:5197–5201.
- Barkou, S. E., J. Broeng, & A. Bjarklev. 1999. Silica-air photonic crystal fiber design that permits waveguiding by a true photonic bandgap effect. *Opt. Lett.* 24:46–49.
- Ctyroky, J., F. Abdelmalek, W. Ecke, & K. Usbeck. 1999a. Modelling of the surface plasmon resonance waveguide sensor with Bragg grating. *Opt. Quantum Electron.* 31:927–941.
- Ctyroky, J., J. Homola, P. V. Lambeck, S. Musa, H. J. W. M. Hoekstra, R. D. Harris, J. S. Wilkinson, B. Usievich, & N. M. Lyndin. 1999b. Theory and modelling of optical waveguide sensors utilising surface plasmon resonance. *Sens. Actuators B* 54:66–73.
- Dostalek, J., J. Ctyroky, J. Homola, E. Brynda, M. Skalsky, P. Nekvindova, J. Spirkova, J. Skvor, & J. Schrofel. 2001. Surface plasmon resonance biosensor based on integrated optical waveguide. *Sens. Actuators B* 76:8–12.
- Diez, A., M. V. Andres, & J. L. Cruz. 2001. In-line fiber-optic sensors based on the excitation of surface plasma modes in metal-coated tapered fibers. *Sens. Actuators B* 73:95–99.
- Engeness, T. D., M. Ibanescu, S. G. Johnson, O. Weisberg, M. Skorobogatiy, S. Jacobs, & Y. Fink. 2003. Dispersion tailoring and compensation by modal interactions in OmniGuide fibers. *Optics Express* 11:1175–1198.
- Gao, Y., N. Guo, B. Gauvreau, M. Rajabian, O. Skorobogata, E. Pone, O. Zabeida, L. Martinu, C. Dubois, & M. Skorobogatiy. 2006. Consecutive solvent evaporation and co-rolling techniques for polymer multilayer hollow fiber preform fabrication. *J. Mat. Res.* 21:2246–2254.
- Grigorenko, A. N., P. Nikitin, & A. V. Kabashin. 1999. Phase jumps and interferometric surface plasmon resonance imaging. *Appl. Phys. Lett.* 75:3917–3919.
- Gupta, B. D., & A. K. Sharma. 2005. Sensitivity evaluation of a multi-layered surface plasmon resonance-based fiber optic sensor: A theoretical study. *Sens. Actuators B* 107:40–49.
- Harris, R., & J. S. Wilkinson. 1995. Waveguide surface plasmon resonance sensors. *Sens. Actuators B* 29:261–267.

- Hassani, A., & M. Skorobogatiy. 2006. Design of the microstructured optical fiber-based surface plasmon resonance sensors with enhanced microfluidics. *Opt. Express* 14:11616–11621. Available on-line at <http://www.opticsinfobase.org/abstract.cfm?URI=oe-14-24-11616>
- Hassani, A., & M. Skorobogatiy. 2007. Design criteria for the microstructured optical fiber-based surface plasmon resonance sensors. *J. Opt. Soc. Am. B* 24:1423–1429.
- Homola, J. 1995. Optical fiber sensor based on surface plasmon resonance excitation. *Sens. Actuators B* 29:401–405.
- Homola, J., R. Slavik, & J. Ctyroky. 1997. Interaction between fiber modes and surface plasmon wave: Spectral properties. *Opt. Lett.* 22:1403–1405.
- Homola, J., J. Ctyroky, M. Skalky, J. Hradiliva, & P. Kolarova. 1997. A surface plasmon resonance based integrated optical sensor. *Sens. Actuators B* 39:286–291.
- Homola, J., S. S. Yee, & G. Gauglitz. 1999. Surface plasmon resonance sensors: Review. *Sens. Actuators B* 54:3–15.
- Jorgenson, R. C., & S. S. Yee. 1993. A fiber-optic chemical sensor based on surface plasmon resonance. *Sens. Actuators B* 12:213–219.
- Kabashin, A. V., & P. Nikitin. 1998. Surface plasmon resonance interferometer for bio- and chemical-sensors. *Opt. Commun.* 150:5–8.
- Kretschmann, E., & H. Raether. 1968. Radiative decay of non radiative surface plasmons excited by light. *Naturforschung A* 23:2135–2136.
- Kuhlmey, B. T., K. Pathmanandavel, & R. C. McPhedran. 2006. Multipole analysis of photonic crystal fibers with coated inclusions. *Opt. Express* 14:10851–10864. Available on-line at <http://www.opticsinfobase.org/abstract.cfm?URI=oe-14-22-10851>
- Lavers, C. P., & J. S. Wilkinson. 1994. A waveguide-coupled surface-plasmon sensor for an aqueous environment. *Sens. Actuators B* 22:75–81.
- Liedberg, B., C. Nylander, & I. Lundstrom. 1983. Surface plasmon resonance for gas detection and biosensing. *Sens. Actuators B* 4:299–304.
- Melendez, J. L., R. Carr, D. U. Bartholomew, K. A. Kukanskis, J. Elkind, S. S. Yee, C. E. Furlong, & R. G. Woodbury. 1996. A commercial solution for surface plasmon sensing. *Sens. Actuators B* 35:212–216.
- Monzon-Hernandez, D., & J. Villatoro. 2006. High-resolution refractive index sensing by means of a multiple-peak surface plasmon resonance optical fiber sensor. *Sens. Actuators B* 115:227–231.
- Monzon-Hernandez, D., J. Villatoro, D. Talavera, & D. Luna-Moreno. 2004. Optical-fiber surface-plasmon resonance sensor with multiple resonance peaks. *Appl. Opt.* 43:1216–1220.
- Murao, T., K. Saitoh, & M. Koshiba. 2006. Design of air-guiding modified honeycomb photonic band-gap fibers for effectively single mode operation. *Opt. Express* 14:2404–2412. Available on-line at <http://www.opticsinfobase.org/abstract.cfm?URI=oe-14-18-8419>
- Piliarik, M., J. Homola, Z. Manikova, & J. Ctyroky. 2003. Surface plasmon resonance based on a polarization-maintaining optical fiber. *Sens. Actuators B* 90:236–242.
- Sheridan, A. K., R. D. Harris, P. N. Bartlett, & J. S. Wilkinson. 2004. Phase interrogation of an integrated optical SPR sensor. *Sens. Actuators B* 97:114–121.
- Skorobogatiy, M. 2005. Efficient anti-guiding of TE and TM polarizations in low-index core waveguides without the need of omnidirectional reflector. *Opt. Lett.* 30:2991–2993.
- Skorobogatiy, M., & A. Kabashin. 2006a. Photon crystal waveguide-based surface plasmon resonance biosensor. *Appl. Phys. Lett.* 89:211641–211643.
- Skorobogatiy, M., & A. Kabashin. 2006b. Plasmon excitation by the Gaussian-like core mode of a photonic crystal waveguide. *Opt. Express* 14:8419–8425.
- Suzuki, H., M. Sugimoto, Y. Matsui, & J. Kondoh. 2006. Fundamental characteristics of a dual-colour fibre optic SPR sensor. *Meas. Sci. Technol.* 17:1547–1552.
- Trouillet, A., C. Ronot-Trioli, C. Veillas, & H. Gagnaire. 1996. Chemical sensing by surface plasmon resonance in a multimode optical fibre. *Pure Appl. Opt.* 5:227–237.
- Tubb, A. J. C., F. P. Payne, R. B. Millington, & C. R. Lowe. 1997. Single-mode optical fibre surface plasma wave chemical sensor. *Sens. Actuators B* 41:71–76.

- Vidal, M. B., R. Lopez, S. Alegret, J. Alonso-Chamarro, I. Garces, & J. Mateo. 1993. Determination of probable alcohol yield in musts by means of an SPR optical sensor. *Sens. Actuators B* 11:455–459.
- Weiss, M. N., R. Srivastava, & H. Grogner. 1996. Experimental investigation of a surface plasmon-based integrated-optic humidity sensor. *Electron. Lett.* 32:842–843.
- Weisser, M., B. Menges, & S. Mittler-Neher. 1999. Refractive index and thickness determination of monolayers by plasmons. *Sens. Actuators B* 56:189–197.
- Zhang, L. M., & D. Uttamchandani. 1988. Optical chemical sensing employing surface plasmon resonance. *Electron. Lett.* 23:1469–1471.